PSIP1/LEDGF reduces R-loops at transcription sites to maintain genome integrity

Sundarraj Jayakumar[1 2], Manthan Patel[1], Fanny Boulet[1], Hadicha Aziz[1], Greg N. Brooke[3], Hemanth Tummala[1] & Madapura M Pradeepa[1*]

1 – Blizard Institute; Faculty of Medicine and Dentistry, Queen Mary University of London, London, UK
2 – Bhabha Atomic Research Centre, Mumbai, India
3 – School of Life Sciences, University of Essex, Colchester, United Kingdom;

[*] Corresponding author Madapura M Pradeepa: p.m.madapura@qmul.ac.uk

Abstract

R-loops that accumulate at transcription sites pose a persistent threat to genome integrity. PSIP1 is a chromatin protein associated with transcriptional elongation complex, possesses histone chaperone activity, and is implicated in recruiting RNA processing and DNA repair factors to transcription sites. Here, we show that PSIP1 interacts with R-loops and other proteins involved in R-loop homeostasis, including PARP1. Genome-wide mapping of PSIP1, R-loops and γ-H2AX in PSIP1-depleted human and mouse cell lines revealed an accumulation of R-loops and DNA damage at gene promoters in the absence of PSIP1. R-loop accumulation causes local transcriptional arrest and transcription-replication conflict, leading to DNA damage. PSIP1 depletion increases 53BP1 foci and reduces RAD51 foci, suggesting altered DNA repair choice. Furthermore, PSIP1 depletion increases the sensitivity of cancer cells to PARP1 inhibitors and DNA-damaging agents that induce R-loop-induced DNA damage. These findings provide fresh insights into the mechanism through which PSIP1 maintains genome integrity at the site of transcription.

Introduction

The newly synthesised nascent RNA can bind to the template DNA during transcription, forming an RNA-DNA hybrid. This hybrid structure combined with the displaced single-stranded DNA is termed R-loops [1]. Physiological R-loops play an essential regulatory role in DNA replication, DNA repair, transcription initiation and termination, and many other cellular processes [2]. On the other hand, accumulating unscheduled R-loops at the site of transcription is known as pathological R-loops. The accumulation of these unscheduled R-loops leads to RNA polymerase-II (RNAPII) pausing and transcriptional arrest [3]. R-loops also cause collision between stalled transcription and replication forks, leading to DNA damage and increased genomic instability [4]. To overcome this, several RNA processing factors (SRSF1), nucleases (RNASEH1 and RNASEH2) and helicases (SETX, DDX1, DDX19 etc.) reduce R-loop levels [2]. Dysregulation of R-loops is linked to neurological autoimmune disorders and cancers (reviewed in) [5]. Intriguingly, R-loops are also accumulated due to DNA double-stranded breaks (DSBs) at the transcription sites. R-loops have also been shown to facilitate DNA repair; however, the mechanism through which R-loops feedback to transcription and DSB repair choice is unclear (reviewed in) [6].

PC4 and SF2 interacting protein (PSIP), also known as LEDGF, is a multifunctional chromatin protein, a proto-oncogene that promotes cell survival, cancer cell proliferation [7–9] and chemotherapy resistance [8,10,11]. PSIP1 binds to methylated histone H3 lysine 36 (H3K36me) via the PWWP domain, and PSIP1 binding is enriched at the sites of RNAPII transcription [12,13]. *PSIP1* encodes two protein isoforms – a shorter PSIP/p52 and a longer PSIP/p75 – generated by alternative splicing (Fig. 1A). The smaller PSIP1/p52 isoform binds to RNA processing proteins and modulates alternative splicing [13]. In contrast, PSIP1/p75 plays a role in guiding the integration of HIV to expressed gene bodies via the interaction of HIV integrase with integrase binding domain (IBD) [14]. PSIP1/75 also interacts with the transcription elongation complex via IBD, which is homologous to the TFIIS N-terminal domain (TFIIS-NTD) (Fig. 1a) [15]. Increased RNAPII pausing and backtracking due to TFIIS mutations results in R-loop formation, leading to genome instability, directly linking transcription stress, R-loop formation, and DNA damage [16]. Interestingly, PSIP1 aids in transcription elongation by functioning as a histone chaperone in the absence of the FACT complex in differentiated cells [17]. It also recruits CtIP to DNA damage sites to promote homologous recombination (HR) at transcribing regions [18,19].

Here, we discovered that PSIP1 interacts with the R-loop directly, and several proteins, including PARP1, are involved in R-loop homeostasis. We also demonstrated that

PSIP1 reduces R-loop levels at the site of RNAPII transcription to maintain genome stability and promotes the repair of DNA damage induced by R-loops by homologous recombination (HR). Furthermore, PSIP1 depletion sensitises cancer cells to clastogens that cause R-loop-induced DNA damage and PARP1 inhibitors.

Results

PSIP1 interacts with R-loops, and PSIP1 depletion elevates the R-loop level

We aimed to investigate the mechanism through which PSIP1 maintains genomic stability. Consistent with the known function of PSIP1 in promoting HDR [19], *Psip1*$^{-/-}$ mouse embryonic fibroblast (MEFs) displayed an elevated number of γ-H2AX foci, a marker of DNA damage (Fig. 1b, Fig. S1A). This increase in DNA damage could be reversed by re-expression of PSIP1/p75, indicating a role of PSIP1/p75 in maintaining genomic integrity in the cells (Fig. 1b). Published proteomics data from immunoprecipitation (IP) of endogenous PSIP1/LEDGF identified several proteins involved in transcription, RNA processing and DNA repair [13,20,21]. Forty-six proteins enriched in the PSIP1 IP overlap with the previously reported S9.6 antibody-based R-loop interactome [22]. These overlapping proteins include DNA-RNA helicases, splicing and DNA repair factors (Fig. S1b). PSIP1 is also enriched among other R-loop modulating proteins in the RNASEH1 TurboID-based proximity-dependent labelling system [23]. Since PSIP1 interacts with RNAPII transcriptional elongation machinery [15] and is associated with transcriptionally active chromatin [13,20], we hypothesised that PSIP1 could prevent R-loop accumulation or promote the resolution of unscheduled R-loops at the sites of RNAPII transcription. We, therefore, sought to investigate whether PSIP1 is involved in R-loop homeostasis.

Firstly, we evaluated the ability of PSIP1 to bind R-loops *in vitro* by incubating the genomic DNA blotted membrane with recombinant PSIP1/p52 and PSIP1/p75, followed by the detection of PSIP1 isoforms using antibodies. Both p75 and p52 isoforms showed binding to R-loops, which was reduced upon RNASEH treatment (Fig. 1c). IP with the S9.6 monoclonal antibody that binds RNA-DNA hybrids (R-loops) [24], detected the interaction of PSIP1/p75 with the R-loop complex. This interaction was abolished upon degradation of R-loops in the RNASEH treated extract (Fig. 1d). Proximity ligation assay (PLA) using S9.6 and PSIP1/p75 antibodies confirmed the interaction of PSIP1/p75 with R-loops (Fig. 1e). Quantifying bulk R-loop levels using immunoblotting of genomic DNA using the S9.6 antibody showed a stark increase in R-loop levels in *Psip1*$^{-/-}$ MEFs compared to the wild type (Fig. 1f). This was rescued upon PSIP1/p75 re-expression, implying the role of PSIP1 in reducing the R-loop level (Fig. 1f). The elevated R-loop levels in *Psip1*$^{-/-}$ MEFs were

sensitive to RNASEH treatment, confirming the specificity of this R-loop detection method (Fig. S1c).

Using two independent short-hairpin (sh) RNAs that target both isoforms of PSIP1, we generated normal prostate epithelial (RWPE-1) and HEK293T cell lines depleted of PSIP1 (PSIP1-KD) (Figs. 1g, S1d and S1g). Immunofluorescence imaging followed by a high-content microscopy and slot blot analysis revealed a significantly higher level of R-loops in the PSIP1-KD compared to the control RWPE-1 nuclei (Fig. 1h) and in HEK293T cells (Fig. S1). RNASEH1 overexpression in these cells led to the reversal of R-loop accumulation (Fig. 1h and Fig. S2a). A similar increase in R-loop intensity was observed when PSIP1 was depleted using an independent shRNA in RWPE-1 cells and HEK293T cells (Fig. S1d–i). Similarly, this increase in R-loop levels mediated by PSIP1 depletion could be rescued by overexpression of p75 or p52 isoforms (Fig. S2b).

To further investigate whether R-loop accumulation is directly due to PSIP1 depletion, we performed two replicates of Cleavage Under Targets and Tagmentation (CUT&Tag) [25], using PSIP1/p75 S9.6 and γ-H2AX antibodies. Reduction in PSIP1/p75 signal in PSIP1-KD cells confirms the specificity of the PSIP1/p75 CUT&Tag data (Figs. 1j). Consistent with the slot blot and immunofluorescence data, we found a nearly five-fold increase in R-loop peaks (n=2741) in PSIP1-KD RWPE-1 cells compared to the control (n=545). Notably, the regions that gained R-loops upon PSIP1 depletion are occupied by PSIP1/p75 in control cells (Figs. 1k and 1l).

PSIP1 depletion leads to increased DNA damage at R-loop sites.

The accumulation of unscheduled R-loops is known to cause DNA replication stress, activating DNA damage response pathways [4]. We found an elevated γ-H2AX level in PSIP1-KD RWPE-1 (Figs. 2a and S3b) and HEK293T cells (Fig. S3a) compared to the control, further confirming the role of PSIP1 in reducing DNA damage. The number of γ-H2AX foci was also significantly higher in PSIP1-depleted RWPE-1 cells. Notably, the increased γ-H2AX foci were reversed upon RNASEH1 overexpression (Fig. 2a and 2b). 53BP1 is crucial to DNA double-strand break (DSB) signalling and repair; the increase in 53BP1 foci and bulk level upon PSIP1 shows increased DNA damage signalling in the absence of PSIP1, which could be rescued by overexpression of RNASEH1 (Figs. 2c and 2d). RNAseq data analysis showed minimal changes in the expression of 186 genes (Supplementary Table.1) implicated in R-loop homeostasis (Fig. S2c). All this evidence indicates that the elevated R-loop levels are due to the PSIP1 depletion but not the indirect consequence of the altered transcriptional programme.

We performed two replicates of CUT&Tag in control and PSIP1 KD HEK293T cells and upon RNASEH1 overexpression. Notably, the elevated S9.6 and γ-H2AX levels in PSIP1 KD could be rescued by RNASEH1 overexpression (Figs. 2e and 2f), confirming the increased DNA damage signalling in PSIP1 KD is due to elevated R-loops. CUT&Tag data is consistent with the increased bulk γ-H2AX level and the number of γ-H2AX foci in the PSIP1-KD (Fig. 2a and 2b). γ-H2AX peaks gained in PSIP1-KD also show an increased R-loop signal (Fig. 2e, 2f and S3c). Furthermore, PLA analysis revealed an increased number and co-localisation of γ-H2AX and R-loop foci in PSIP1-KD, further confirming that R-loops accumulated upon PSIP1 depletion are responsible for increased DNA damage in PSIP1 KD (Fig. 2g).

R-loops cause transcriptional arrest and transcription-replication conflict.

CUT&Tag with γ-H2AX antibodies revealed an increase in the number of γ-H2AX peaks in PSIP1 KD compared to control (Fig. 3a). Notably, PSIP/p75 is enriched at γ-H2AX peaks specific to PSIP1-KD, confirming that γ-H2AX accumulation is due to the direct consequence of PSIP1 depletion (Figs. 3b and c). R-loop peaks gained, as a result of PSIP1-KD, were enriched around promoter or transcription start sites (TSS) and gene bodies compared to intergenic regions (Fig. 3a). Similarly, PSIP1/p75 binding showed enrichment around gene promoters, PSIP1 depletion led to an increase in R-loop levels and DNA damage (γ-H2AX level) at PSIP1 binding sites (Fig. 3a–3c). Peak overlap analysis revealed that the 909 R-loop peaks detected in PSIP KD overlapped with PSIP1/p75 peaks in control cells. Similarly, 239 S9.6 and γ-H2AX peaks that appeared upon PSIP1 depletion overlapped with the PSIP1/p75 peaks in control (Fig. 3c). Accumulated R-loops show enrichment for G-rich promoters with high GC skew, suggesting that PSIP1 reduces R-loops at G-rich promoters or genes regulated by strong CpG islands with high transcriptional activity (Fig. S4a and S4b) [26].

R-loops can induce transcriptional termination or arrest [27,28]. To investigate whether R-loop accumulation upon PSIP1 depletion affects transcription at the sites of R-loop accumulation, we performed transient transcriptome sequencing (TT-seq) by labelling newly synthesised transcripts with 4SU [29]. Meta-analysis of TT-seq data showed an overall reduced level of nascent transcription across the gene transcription unit. The reduction in TT-seq signal was higher at the promoter or upstream of gene TSS compared to the rest of the gene body (Fig 3d). Replotting of TT-seq reads at R-loops that are gained in PSIP KD revealed a stark reduction in the nascent transcript levels (Fig. 3d). Furthermore, triptolide-mediated transcription inhibition reversed the elevated R-loop levels in PSIP1-KD (Fig. 3e). These

results suggest the role of PSIP1 in reducing the R-loop level during ongoing transcription, accumulation of these R-loops, which can otherwise lead to transcriptional arrest. However, since PSIP1 is a transcriptional regulator, it is tricky to infer the direct effect of PSIP1 depletion on R-loop mediated transcriptional arrest.

The R-loop-induced transcriptional arrest can cause collisions with the DNA replication forks, resulting in DNA damage. R-loop accumulation in the head-on orientation with the replication fork can cause a transcription-replication conflict (TRC) [4]. Hence, we monitored the interaction between the transcription and replication machinery using the PLA for RNAP II and PCNA antibodies, which mark transcription complexes and replication forks. Increased RNAPII and PCNA PLA foci in PSIP1 KD show a higher level of TRC in the absence of PSIP1; RNASEH1 overexpression in the PSIP1 KD leads to significantly reduced RNAPII and PCNA PLA foci suggesting reduced TRC due to rescue in elevated R-loops (Fig. 3f). Reduced incorporation of 5-ethynyl-2'-deoxyuridine (EdU) into DNA in PSIP1-KD in an EdU incorporation assay implies a slower replication rate upon PSIP depletion (Fig. S5a). Cell cycle analysis revealed that reduced EdU incorporation is not due to changes in the cell cycle stages due to PSIP1 depletion (Fig. S5b). These results show that PSIP1 reduces transcription-induced R-loops, which can otherwise lead to local transcriptional arrest due to collision with the replication fork, resulting in reduced replication.

PSIP1 promotes the repair of DNA damage induced by transcription and R-loops

Our data showed increased DNA damage upon PSIP1 depletion is due to elevated R-loops (Fig. 3b-3f). The slow repair of R-loop induced DNA damage could also contribute to the observed increase in DNA damage. The absence of PSIP1 could slowdown repair of R-loop mediated DNA damage, as PSIP1 is known to promote HR [19], and interacts with DNA repair factors (Fig. S1b). The DNA damage caused by R-loops is repaired by transcription-coupled double-strand break repair [30]. To investigate the role of PSIP1 in the repair of R-loop mediated DNA damage at the site of transcription, we treated the cells with illudin-S and etoposide, which are known to cause transcription-coupled DNA damage. PSIP1 depletion led to an increased sensitivity to illudin-S mediated DNA lesions that are specifically repaired by the transcription-coupled nucleotide excision repair (TC-NER) pathway but not global nonhomologous end joining (NHEJ) and base excision repair (BER) [31]. Similarly, PSIP1 depletion increased sensitivity to etoposide, which is known to bind topoisomerase II and block transcription and replication [32] (Fig. 4a). Phleomycin treatment, which induces DSBs showed similar sensitivity, but not aphidicolin that causes cell cycle arrest [33,34] (Fig. S6b and

Fig. 4a). This specific sensitivity to clastogens, that interfere with the transcription process, reveals the role of PSIP1 in promoting DNA repair at the site of transcription. Further, western blotting for γ-H2AX revealed a sustained DNA damage response in phleomycin-treated PSIP1-KD compared to the control cells (Fig. 4b).

Enrichment of PSIP1/p75 in γ-H2AX IP shows that PSIP1 is recruited to DNA damage sites (Fig. 4c). Notably, PSIP1 recruitment to γ-H2AX sites is further increased when treated with camptothecin (CPT), which induces R-loop formation (Fig. 4c, S6d and S6e) by inhibiting topoisomerase 1 (TOP1) at active promoters [35]. However, PSIP1 recruitment to γ-H2AX chromatin was reduced upon overexpression of RNASEH1 (Fig. 4c). The protein level of DNA-PK, which is involved in the NHEJ pathway, is increased in PSIP1-KD cells (Fig. 4b). Similarly, the number of 53BP1 (known to promote NHEJ) foci, were significantly higher in PSIP1-KD and upon CPT treatment compared to the control (Figs. 4d and e). A similar increase in 53BP1 foci was also observed after phleomycin treatment in PSIP1-KD (Fig. S6c). In contrast, the number of RAD51 foci, a marker of the HR pathway, was significantly reduced (Fig. 4e). These results agree with the role of PSIP1 in promoting the HR repair pathway [18,19]. These results suggest that PSIP1 facilitates the repair of R-loop mediated DNA damage through the HR pathway at the transcription sites.

Reduced PSIP1 levels sensitise cancer cells to transcription-induced DNA damage.

PARP1 is a vital DNA repair factor and also an R-loop resolving factor. Since PARP1 was one of the significant interactors with PSIP1/p75 and was also enriched in the R-loop proteome [21,22] (Fig. S1b), we further confirmed the interaction of PARP1 and PSIP1 with the R-loops by S9.6 antibody IP (Fig. 5a). Reciprocal α-PSIP1-IP performed in the presence of benzonase (a universal nuclease, which degrades both RNA and DNA) (Fig. 5b), together with co-IP of HA-tagged PSIP1/p75 and PSIP1/p52 with GFP-tagged PARP1 confirmed the interaction between both PSIP1 isoforms with PARP1, along with γ-H2AX (Fig. 5c). Comparison of the PSIP1 transcripts across different cancer types in the TCGA database revealed lower PSIP1 levels compared to the respective control tissues (Fig. 5d). Cells with elevated levels of R-loops are sensitive to PARP1 inhibitor-induced cell death [36]. Hence, we aimed to investigate whether cancers with low PSIP1 levels are sensitive to PARP1 inhibitors or illudin-S that cause transcription-coupled DNA damage. Prostate cancer cell lines (LNCaP and PC3) showed lower levels of PSIP1 compared to normal prostate epithelial cells (RWPE-1) (Fig. 5e). These prostate cancer cells showed significantly higher sensitivity to the PARP1 inhibitor (PARPi) olaparib compared to RWPE-1 cells (Fig. 5f). PSIP1 depletion in LNCaP cells increased olaparib sensitivity, which could be partially rescued by RNASEH1

overexpression (Figs. 5g and 5h). These results show that PSIP1 and PARP1 synergistically reduce R-loops-induced genomic instability. Depletion of PSIP1 also led to hypersensitivity of LNCaP cells to illudin-S, which was reversible by RNASEH1 overexpression (Fig. 5i). These data suggest that the clastogens and PARP1 inhibitors that are known to interfere with the transcription-coupled DNA repair mechanism, could be effective in inducing synthetic lethality in specific cancers.

Discussion

Accumulation of unscheduled co-transcriptional R-loops affects transcription elongation, compromises genome integrity, and is implicated in cancer and inflammation. Here, we demonstrate that PSIP1 binds to R-loops and proteins associated with R-loops, including PARP1. PSIP1 reduces R-loops formed during transcription to minimise DNA damage and genomic instability (Fig. 5J). R-loops and γ-H2AX accumulation are sensitive to inhibition of transcription and overexpression of RNASEH1, which confirms the elevated DNA damage in PSIP1-KD cells due to unresolved R-loops that appear at the site of transcription. Furthermore, PSIP1/p75 R-loops are detected at promoters and gene bodies, confirming the role of PSIP1 in resolving transcription-induced R-loops. We further demonstrate that elevated DNA damage is due to R-loop-induced collision between RNAPII transcription with the replication fork (Fig. 5j).

PSIP1 isoforms are enriched at the transcription unit of expressed genes through binding to di and tri-methylated H3K36 [13,37]. Recently, PSIP1 have been shown to function as a histone chaperone in the absence of the FACT complex in differentiated cells to facilitate transcriptional elongation through nucleosomes [17]. Interestingly, FACT complex subunits (SSRP1 and SPT16) are detected in the R-loop and PSIP1/p75 interactome, also known to aid the R-loop resolution [21,22,38]. The intrinsic transcript-cleavage activity of RNAPII requires TFIIS to suppress R-loop formation by reducing RNAPII pausing and backtracking [28]. Intriguingly, PSIP1/p75 also has a TFIIS N-terminal domain that interacts with the transcription elongation complex [15]. These pieces of evidence suggest a broader role of histone chaperones in facilitating transcriptional elongation by reducing R-loops formed at the transcription site. Several R-loop resolving proteins such as TFIIS, PSIP1, PARP1, FACT complex, and topoisomerases are shown to function in efficient transcriptional elongation [22,38–42]. It is plausible that PSIP1 restrains the transcription elongation when it encounters R-loop mediated DSBs to facilitate the resolution of R-loop and promote HR-mediated DNA repair[18,43], as PSIP1 is also known to restrain transcription elongation [20].

Several proteins involved in transcription, RNA processing and DNA repairs, such as the PARP1, TFIIS, BRCA1, THO complex, SRSF1, DDX23, SETX, DHX9, TOP1 and others, are known to reduce R-loop burden and genome instability [3,44–47]. Interestingly, the splicing factor SRSF1, one of the significant interacting partners of PSIP1, also reduces the genomic instability caused by R-loops [48]. Further investigation will be needed to test whether the R-loops, elevated upon PSIP1 depletion, are due to dysregulated RNA processing due to reduced recruitment of splicing factors [49].

The unscheduled R-loops can induce transcriptional repression via various mechanisms [50]. DNA damage-induced transcriptional arrest is essential to prevent replication and transcription collision due to aberrant transcripts, which could also generate R-loops [51]. Reduced nascent transcript levels at R-loop sites and increased PLA foci between PCNA and RNAPII show that unresolved R-loops lead to increased transcription-replication conflict (TRC). Although most PSIP1 binding and PSIP1-KD-specific R-loops are detected around promoters and gene bodies, intergenic regions also show enrichment for R-loops and γ-H2AX. Although most of the R-loops and DNA damage were detected at gene transcription units, distal regulatory elements are also a source of enhancer RNA transcription that could lead to R-loops and DSBs [52].

The interaction of PSIP1/p75 with CtIP and various DNA repair factors also suggests its role in promoting HR and improving the efficiency of DNA repair during transcription [19,21,53]. PSIP1 promotes HR in transcribing regions [18,19]. PARP1 inhibitors are successfully used for cancers deficient in HR due to *BRCA* mutations [54]. Importantly, our data show that depletion of PSIP1 results in higher sensitivity of prostate cancer cells to clastogens that cause transcription-coupled DNA damage and a PARP1 inhibitor. Although PSIP1-KD sensitised cancer cells to clastogens, including PARPi, further studies are needed to validate their efficacy *in vivo*. Since we detect accumulation of both R-loops and DNA damage in the absence of PSIP1, some of the R-loops accumulated in the PSIP1-KD could be due to DNA damage, as double-stranded breaks are known to generate R-loops [55].

In summary, we show that PSIP1 interacts with proteins involved in the R-loop homeostasis, such as DNA repair, RNA processing factors, and PARP1. PSIP1 maintains genomic stability at the site of transcription by a) reducing the R-loop levels by interacting or recruiting R-loop processing proteins and b) promoting the HR repair pathway to repair damage caused by transcription-induced R-loops. Our data also revealed an increased sensitivity of cancer cells with low levels of PSIP1 to drugs that induce transcription-associated DNA damage and PARP1 inhibitors. With further *in vivo* validations, insights

from this work could be used to therapeutically target cells with higher R-loop levels, therefore having significant implications for diseases such as cancer.

Methods

Materials:

The materials used in the study and the details are listed in the Supplementary Table. 2.

Cell culture

RWPE-1, PC-3, LNCaP and HEK293T cells were procured from American Type Culture Collection. *Psip1*$^{-/-}$ and its corresponding WT MEFs were a kind gift from Prof. Alan Engelman (Dana-Farber Cancer Institute, USA) [47]. The *Psip1*$^{-/-}$ P75 rescue cells were generated in the lab by expressing lentiviral with P75 cDNA [48]. RWPE-1 cells were cultured in a K-SFM medium. LNCaP cells were cultured in an RPMI medium. PC-3, HEK293T and MEF cells were cultured in a DMEM medium. The medium was supplemented with 1X penicillin, streptomycin solution, and 10 % FBS. Cells are grown as an adherent monolayer culture in the appropriate medium, in the incubator at 37°C and 5% CO_2.

Generation of PSIP1 knock-down cell lines

Lentiviral shRNA vectors targeting PSIP1 (PSIP1 ShRNA1 TRCN0000298567, PSIP1 shRNA2 TRCN0000286345) and non-targeting control were procured from Sigma Life Sciences. Exponentially growing cells were transduced with lentivirus; 24 h after the transduction media was changed, cells were selected for stable integration using puromycin antibiotic selection at the following concentration: RWPE-1- 3ug/ml; HEK293T, PC-3 and LNCaP: 2 ug/ml.

R-loop slot blot

R-loops were estimated by slot blot as described in [22]. Cells were lysed in lysis buffer (100 mM Tris-HCl (pH 8.5), 5 mM EDTA, 0.2% SDS, 100 mM NaCl, proteinase K 0.5 mg/ml) and incubated at 55°C overnight. Ice cold isopropanol was added to the lysate, and the RNA-DNA was pelleted using centrifugation (12000 RPM; 4°C). The ellet was washed once with 70% ethanol, and the pellet was dissolved in TE buffer. The RNA-DNA was quantified using a nanodrop spectrophotometer by taking the absorption at 260 nm. Based on the quantification, different quantities (500, 250 and 125 ng) of DNA were blotted onto the N+ nitrocellulose membrane using a slot blot apparatus. For RNASEH digestion, 2 µg of RNA-DNA was incubated with 5 units of RNASEH at 37°C for 20 min and they were used for slotting on the membrane. The membrane was baked at 80°C for 2h, incubated in blocking buffer (5% skimmed milk in PBS) for 1 hour, followed by incubation with S9.6 antibody (1:1000 dilution) overnight at 4°C in a nutator. Blots were washed three times with PBST (5

min each), incubated with secondary antibody (1:1500 dilution) for 2h at room temperature, followed by three washes in PBST 3 times (5 min each) and developed with the ECL reagents A and B (Cell signalling Technology cat no: 46935P3 and 74709P3). The same blots were stained with methylene blue to quantify total DNA.

Determining PSIP1 binding with R-loops

To determine the binding of PSIP1 isoforms (p75 and p52) to R-loops, DNA with R-loops was extracted from HEK293T cells using the steps described in the previous section. The isolated DNA was slotted onto the membrane, blocked using 5% skimmed milk and then the membrane was incubated with either p75 protein (150 ng in 3 ml of 5% skimmed milk), or p52 protein (150 ng in 3 ml of 5% skimmed milk) or IgG protein (as control) overnight at $4^{o}C$ in a nutator. Then the membrane was washed three times with PBST solution (5 min each) and incubated with antibody (1:1000 dilution) specific to p75, p52 and IgG (incubation O/N at $4^{o}C$ in a nutator). The membranes were washed three times again using PBST and incubated with HRP coupled secondary antibody (1:1500 dilution) and the blots were developed with ECL reagents as described in the previous section.

Immunoprecipitation

The cells were grown to ~90 % confluency, washed with PBS, treated with hypotonic solution (10 mM Tris pH 8.0, 1.5 mM MgCl2, 10 mM KCl, 0.5 mM DTT, Protease inhibitor cocktail), scrapped from the dish using a cell scrapper, and collected in the centrifuge tubes. The nuclear pellet was isolated, and the nuclear extract was prepared using NP-40 lysis buffer (50 mM Tris-HCl pH 8.0, 150 mM KCl, 1% NP-40, 1.5 mM MgCl2, 0.1 mM DTT, 0.2 mM EDTA

And Protease Inhibitor Cocktail). The nuclear extract was subjected to pre-clearing by incubating 500 µl of nuclear lysate with 50 µl of Protein-A Dynabeads ($4^{o}C$ in a nutator for 1 h). After removal of the beads, a part of the lysate was aliquoted as the input control and the remaining lysate was incubated with the specified primary antibody (5 µg of antibody for 500 µl of nuclear lysate) overnight at $4^{o}C$. Washed Protein-A Dynabeads were added to the lysate, incubated at $4^{o}C$ for 1 h, and pulled down using the magnet. The supernatant was discarded, and the beads were washed three times (10 min each) with NP-40 lysis buffer. The proteins bound to the beads were extracted using a Bolt Nupage 4X sample loading buffer and loaded onto the gel for the detection of different proteins by western blotting.

Western blotting

For western blotting, cells were harvested, pelleted, washed with PBS once and lysates were prepared using RIPA buffer (50 mM Tris, pH 8.0, 150 mM NaCl, 1% NP-40, 0.5% Sodium deoxycholate, 0.1% SDS, protease inhibitors and Benzonase; incubation on ice for 30 min with brief sonication for 5 min). Extracts were cleared by centrifugation at 13000 RPM for 10 min at 4°C, sample buffer, reducing agents were added and the lysate was boiled for 5 min in a boiling water bath before cooling on ice. The sample lysates were loaded onto the True-PAGE precast gels and were subjected to electrophoresis at 95 V for 90 min. Proteins were transferred to the PVDF membrane using a Trans-blot turbo transfer system (Bio-Rad). Membranes were blocked with every blot blocking buffer (Bio-Rad), incubated with primary antibody (~1:1000 dilution in blocking buffer) overnight at 4°C, followed by three washes with 0.05% PBST, incubated with HRP coupled secondary antibodies (1:1500 dilution in blocking buffer) for 2h at room temperature, followed by three times wash with 0.05% PBST. Membranes were developed with ECL reagents.

Proximity Ligation Assay (PLA)

Control and PSIP1-KD RWPE1 cells were seeded in 96 well plates (glass bottom). PLA was performed using Duolink In Situ Red Starter kit (Mouse/Rabbit) according to the manufacturer protocol (Merck, DUO92101).

Clonogenic assay

Five hundred cells for each cell type were plated in triplicates for each treatment per well in a 6-well plate. The cells were allowed to grow and develop colonies for 10-14 days after the treatment of the indicated drugs. The colonies were washed and fixed with methanol, stained with crystal violet, and counted manually to calculate the survival fraction using the following formula. Survival fraction = plating efficiency of treatment/plating efficiency of control X 100.

Immunofluorescence

For immunofluorescence of R-loops, the exponentially growing cells were washed once with PBS and fixed using cold methanol at -20°C for 15 min. For immunofluorescence of γ-H2AX and 53BP1, fixin of the cells was done using 4% para-formaldehyde for 20 min. After fixation, the cells were washed with PBS, permeabilised using 0.3% Triton-X-100, blocked using 3% BSA for 1 h, and incubated with primary antibody (1:250 dilution) at 4°C for overnight. After washing with PBST three times, the cells were incubated with secondary antibodies conjugated to different fluorophores (1:750 dilution) and were imaged in the laser-based InCell high-content imaging system (IN Cell Analyzer 6000, GE Healthcare). The nuclear levels of S9.6 or the number of γ-H2AX foci was quantified using the INCarta

software that is attached to the imaging system. Fluorescence from 3000-5000 cells were used for quantification and were plotted using Graphpad Prism 9.0 software. The same slides were also visualised in Zeiss 880 Laser Scanning Confocal Microscope and images were grabbed.

Plasmid overexpression

For overexpression of pEGFP-RNASEH1 (Addgene ID 108699, a kind gift from Martin Reigns, MRC-HGU, Edinburgh) [49], HA-p75-IRES-GFP, HA-p52-IRES-GFP plasmids in PSIP1 KD cells, FuGENE® HD Transfection Reagent (Promega) was used as per the manufacturers instruction. In control cells, mock transfection was performed using IRES-GFP plasmids. The transfection efficiency was verified using the expression of GFP. Thirty-six hours after transfection, cells were used for further experiments.

CUT&Tag

CUT&Tag was performed according to [50] protocol with modifications to tissue processing as described below. Experiments were performed in biological duplicates from each cell type. ~100,000 cells were pelleted by centrifugation for 3 min at 600 x g at room temperature and resuspended in 500µl of ice-cold NE1 buffer (20 mM HEPES-KOH pH 7.9, 10 mM KCl, 0.5 mM spermidine, 1% Triton X-100, and 20 % glycerol and cOmplete EDTA free protease inhibitor tablet) and was let to sit for 10 min on ice. Nuclei were pelleted by centrifugation for 4 min at 1300 x g at 4°C, resuspended in 500µl of wash buffer and held on ice until beads were ready. The required amount of BioMag Plus Concanavalin-A-conjugated magnetic beads (ConA beads, Polysciences, Inc) were transferred into the binding buffer (20 mM HEPES-KOH pH 7.9, 10 mM KCl, 1mM $CaCl_2$ and 1mM $MnCl_2$), washed once in the same buffer, each time placing them on a magnetic rack to allow the beads to separate from the buffer and resuspended in binding buffer. 10 µl of beads was added to each tube containing cells and rotated on an end-to-end rotator for 10 minutes. After a pulse spin to remove liquid from the cap, tubes were placed on a magnet stand to clear, the liquid was withdrawn, and 800 µl of antibody buffer containing 1 µg of primary antibodies was added and incubated at 4 ºC overnight in a nutator. Secondary antibodies (guinea pig α-rabbit antibody, Antibodies online, ABIN101961 or α-mouse antibodies) were diluted 1:100 in dig-wash buffer (5% digitonin in wash buffer), and 100 µL was added in per sample while gently vortexing to allow the solution to dislodge the beads from the sides and incubated for 60 min on a nutator. Unbound antibodies were washed in 1 ml of dig-wash buffer three times. 100 µl of (1:250 diluted) protein-A-Tn5 loaded with adapters in dig-300 buffer (20 mM HEPES pH 7.5, 300

mM NaCl, 0.5 mM spermidine with Roche cOmplete EDTA free protease inhibitor) was added to the samples, placed on nutator for 1 hour and washed three times in 1 ml of dig-300 buffer to remove unbound pA-Tn5. 300 µL tagmentation buffer (Dig-300 buffer + 5 mM $MgCl_2$) was added while gentle vortexing, and samples were incubated at 37ºC for 1 hr. Tagmentation was stopped by adding 10 µL 0.5M EDTA, 3 µL 10% SDS and 2.5 µL 20 mg/mL Proteinase K to each sample. Samples were mixed by full-speed vortexing for ~2 seconds and incubated for 1 hr at 55ºC to digest proteins. DNA was purified by phenol: chloroform extraction using phase-lock tubes (Quanta Bio) followed by ethanol precipitation. Libraries were prepared using NEBNext HiFi 2x PCR Master mix (M0541S) with a 72ºC gap-filling step followed by 13 cycles of PCR with 10-second combined annealing and extension to enrich short DNA fragments. Libraries were sequenced in Novaseq 6000 (Novogene) with 150bp paired-end reads. For HEK293T CUT&Tag, we followed the following protocol https://www.protocols.io/view/cut-amp-tag-direct-for-whole-cells-with-cutac-x54v9mkmzg3e/v4.

Transient transcriptome sequencing (TT-seq)

TT-seq was performed according to the protocol described in [51] with modifications including CORALL total RNAseq library preparation kit (Lexogen Cat. no. 147.24) was used for library preparation, followed by sequencing.

CCK-8 –assay

Seven thousand cells were plated on a 96-well plate for overnight attachment. The next day, cells were added with different drug concentrations and cultured for 48h in the incubator. Fresh media containing 50ug/ml of WST-8 dye was replaced and incubated for 1h. Then the absorbance was recorded at 450 nm, and the absorbance value was used to calculate the percentage of viable cells.

EdU incorporation assay

EdU incorporation was performed using Click-iT™ Plus EdU Alexa Fluor™ 647 Assay Kit (Invitrogen). EdU (5-ethynyl-2'-deoxyuridine, 20 mM) was added to the culture dishes with cells and grown for 4 hours. Then, cells were fixed using 3.8% formaldehyde for 15 min at room temperature and washed twice with 3% BSA in PBS. Cells were permeabilised using 0.5% Triton-X-100 (20 min) and stained using the Click-iT cocktail following the vendor's protocol. Cells were imaged under IN Cell Analyzer 2200 (GE Healthcare Life Sciences), and the fluorescent intensity was quantified (from at least 5000 cells) using IN Carta Image Analysis Software (Molecular Devices).

Cell cycle analysis by flowcytometry

The exponentially growing cells were harvested, stained with DAPI and cells were acquired using ACEA Novocyte 3000 flow cytometer. The cell cycle analysis was performed using NovoExpress Software attached to the machine.

Data Analysis:

CUT&Tag

The pair-end sequencing reads generated for the CUT&Tag were trimmed for the sequencing adapters with a trimmomatic tool, followed by mapping onto the human genome hg38 using *bowtie2*. The reads were aligned using following parameters: *--very-sensitive-local --no-unal --no-mixed --no-discordant --phred33 -I 10 -X 700*. The data was processed using SAMtools to generate bam files and sort them. All the replicates were pooled using *SAMtools merge*. Merged bam files were used to generate bed files, bedgraph and bigwig.

Peak calling

Peaks on the mapped reads were called using the *SEACR* tool using IgG as a background with *"norm and relaxed"* options. For each replicate, the peaks were called using both individual IgG replicates as background. The peaks obtained were pooled, only the peaks consistent in both replicates were retained, and coordinates were merged. These peaks were used for further analyses.

Peaks were processed using the *bedtools intersect* option to filter the peaks unique to either WT (PSIP peaks) or KD (γ-H2AX and S9.6 peaks). Peak distribution across genomic landmarks (TSS, gene body or intergenic) was done on the coordinates obtained from the UCSC genome browser using *bedtools intersect*.

Bigwig generation and plotting

The signal files for merged samples were generated using the deepTools bamCoverage option with the following parameters: *--binSize 20 –normalise Using CPM --scaleFactor --smoothLength 60 --extended 150 –centerReads*. The signal was normalised between WT and KD for each target by comparing the reads mapping to the *E. coli* genome. The bigwigs generated were used for viewing on the genome browser or plotting as a heatmap or average summary plot on the genomic landmarks and peaks. Matrices generated through *computeMatrix* with *reference-point or scale-region option* were used as input for heatmap *(plotHeatmap) or* average summary *(plotProfile), or* violin *(R package ggplot2)* plots. The genome browser views were captured on the UCSC genome browser.

RNAseq and TTseq

Pair-end reads for the RNA-seq, and TT-seq were aligned against the human genome (hg38) via STAR aligner following the Bluebee-CORALL mapping pipeline. The replicates were

merged for each sample using SAMtools merge, followed by filtering out the multi-mapped reads by defining MAPQ as 255. The bigwigs were generated using the deepTools bamCoverage tool with the option to normalise using RPKM. These bigwigs were used for comparing the signal in the genome browser or plotting heatmaps, average summary plots or violin plots on the genes and peaks datasets. Differential gene expression for the RNAseq was performed through the DESeq2 package. The fragments count matrix was generated using the Subreads feature counts option. This count matrix was subjected to DESeq2, and the result obtained from the analysis was used to plot as a Volcano plot.

GC skew analysis

GC skew for the S9.6, PSIP1 and γ-H2AX CUT&Tag peaks was calculated using the ratio of (G-C)/(G+C). The values were used to plot the frequency distribution. For the background frequency of the GC skew, randomly shuffled genomic coordinates were used to compare it. Further, the PSIP1, S9.6 and γ-H2AX signal distribution was compared on the GC-skewed regions of our genome [25]. The coordinates were lifted from hg18 to hg38 and used for plotting. Likewise, the signal was also plotted for the G-rich promoters [25].

Data availability: The data discussed in this publication have been deposited in NCBI's Gene Expression Omnibus (Sundarraj et al., 2023) and are accessible through GEO Series accession number GSE 220234:
Go to https://www.ncbi.nlm.nih.gov/geo/query/acc.cgi?acc=GSE220234

Code availability

No custom codes are used in this study

References

1. Petermann, E., Lan, L. & Zou, L. Sources, resolution and physiological relevance of R-loops and RNA-DNA hybrids. *Nat. Rev. Mol. Cell Biol.* **23**, 521–540 (2022).
2. García-Muse, T. & Aguilera, A. R Loops: From Physiological to Pathological Roles. *Cell* **179**, 604–618 (2019).
3. Chen, L. *et al.* The Augmented R-Loop Is a Unifying Mechanism for Myelodysplastic Syndromes Induced by High-Risk Splicing Factor Mutations. *Mol. Cell* **69**, 412-425.e6 (2018).
4. Hamperl, S., Bocek, M. J., Saldivar, J. C., Swigut, T. & Cimprich, K. A. Transcription-Replication Conflict Orientation Modulates R-Loop Levels and Activates Distinct DNA Damage Responses. *Cell* **170**, 774-786.e19 (2017).
5. Brickner, J. R., Garzon, J. L. & Cimprich, K. A. Walking a tightrope: The complex balancing act of R-loops in genome stability. *Mol. Cell* **82**, 2267–2297 (2022).
6. Marnef, A. & Legube, G. R-loops as Janus-faced modulators of DNA repair. *Nat. Cell Biol.* **23**, 305–313 (2021).
7. Bhargavan, B. *et al.* LEDGF gene silencing impairs the tumorigenicity of prostate cancer DU145 cells by abating the expression of Hsp27 and activation of the Akt/ERK signaling pathway. *Cell Death Dis.* **3**, e316 (2012).
8. French, J. D. *et al.* Germline polymorphisms in an enhancer of PSIP1 are associated with progression-free survival in epithelial ovarian cancer. *Oncotarget* **7**, (2016).
9. Singh, D. K. *et al.* PSIP1/p75 promotes tumorigenicity in breast cancer cells by promoting the transcription of cell cycle genes. *Carcinogenesis* **38**, 966–975 (2017).
10. Basu, A. *et al.* LEDGF/p75 overexpression attenuates oxidative stress-induced necrosis and upregulates the oxidoreductase ERP57/PDIA3/GRP58 in prostate cancer. *PLoS One* **11**, 1–25 (2016).
11. Ríos-Colón, L. *et al.* Targeting the stress oncoprotein LEDGF/p75 to sensitize chemoresistant prostate cancer cells to taxanes. *Oncotarget* **8**, 24915–24931 (2017).
12. Nuland, R. Van *et al.* Nucleosomal DNA binding drives the recognition of H3K36-methylated nucleosomes by the PSIP1-PWWP domain. *Epigenetics and Chromatin* **6**, 1–12 (2013).

13. Pradeepa, M. M., Sutherland, H. G., Ule, J., Grimes, G. R. & Bickmore, W. A. Psip1/Ledgf p52 binds methylated histone H3K36 and splicing factors and contributes to the regulation of alternative splicing. *PLoS Genet.* **8**, e1002717 (2012).
14. Marshall, H. M. *et al.* Role of PSIP1/LEDGF/p75 in lentiviral infectivity and integration targeting. *PLoS One* **2**, e1340 (2007).
15. Cermakova, K. *et al.* A ubiquitous disordered protein interaction module orchestrates transcription elongation. *Science* **374**, 1113–1121 (2021).
16. Zatreanu, D. *et al.* Elongation Factor TFIIS Prevents Transcription Stress and R-Loop Accumulation to Maintain Genome Stability. *Mol. Cell* **76**, 57-69.e9 (2019).
17. LeRoy, G. *et al.* LEDGF and HDGF2 relieve the nucleosome-induced barrier to transcription. *Sci. Adv.* **5 : eaay30**, (2019).
18. Aymard, F. *et al.* Transcriptionally active chromatin recruits homologous recombination at DNA double-strand breaks. *Nat. Struct. Mol. Biol.* **21**, 366–374 (2014).
19. Daugaard, M. *et al.* LEDGF (p75) promotes DNA-end resection and homologous recombination. *Nat. Struct. Mol. Biol.* **19**, 803–10 (2012).
20. Pradeepa, M. M., Grimes, G. R., Taylor, G. C. a, Sutherland, H. G. & Bickmore, W. a. Psip1/Ledgf p75 restrains Hox gene expression by recruiting both trithorax and polycomb group proteins. *Nucleic Acids Res.* **42**, 9021–32 (2014).
21. Sundarraj, J., Taylor, G. C. A., von Kriegsheim, A. & Pradeepa, M. M. H3K36me3 and PSIP1/LEDGF associate with several DNA repair proteins, suggesting their role in efficient DNA repair at actively transcribing loci. *Wellcome Open Res.* **2**, 83 (2021).
22. Cristini, A., Groh, M., Kristiansen, M. S. & Gromak, N. RNA/DNA Hybrid Interactome Identifies DXH9 as a Molecular Player in Transcriptional Termination and R-Loop-Associated DNA Damage. *Cell Rep.* **23**, 1891–1905 (2018).
23. Yan, Q. *et al.* Proximity labeling identifies a repertoire of site-specific R-loop modulators. *Nat. Commun.* **13**, 1–17 (2022).
24. Boguslawski, S. J. *et al.* Characterization of monoclonal antibody to DNA.RNA and its application to immunodetection of hybrids. *J. Immunol. Methods* **89**, 123–130 (1986).
25. Wang, K. *et al.* Genomic profiling of native R loops with a DNA-RNA hybrid recognition sensor. *Sci. Adv.* **7**, (2021).
26. Ginno, P. A., Lott, P. L., Christensen, H. C., Korf, I. & Chédin, F. R-Loop Formation Is a Distinctive Characteristic of Unmethylated Human CpG Island Promoters. *Mol.*

Cell **45**, (2012).

27. Skourti-Stathaki, K. *et al.* R-Loops Enhance Polycomb Repression at a Subset of Developmental Regulator Genes. *Mol. Cell* **73**, 930-945.e4 (2019).
28. Zatreanu, D. *et al.* Elongation Factor TFIIS Prevents Transcription Stress and R-Loop Accumulation to Maintain Genome Stability. *Mol. Cell* **76**, 57-69.e9 (2019).
29. Schwalb, B. *et al.* TT-seq maps the human transient transcriptome. *Science (80-.).* **352**, 1225–1228 (2016).
30. Cohen, S. *et al.* A POLD3/BLM dependent pathway handles DSBs in transcribed chromatin upon excessive RNA:DNA hybrid accumulation. *Nat. Commun.* **13**, 2012 (2022).
31. Jaspers, N. G. J. *et al. Anti-tumour compounds illudin S and Irofulven induce DNA lesions ignored by global repair and exclusively processed by transcription-and replication-coupled repair pathways*. *DNA Repair* vol. 1 (2002).
32. Montecucco, A., Zanetta, F. & Biamonti, G. Molecular mechanisms of etoposide. *EXCLI J.* **14**, 95–108 (2015).
33. Krokan, H., Wist, E. & Krokan, R. H. Aphidicolin inhibits DNA synthesis by DNA polymerase alpha and isolated nuclei by a similar mechanism. *Nucleic Acids Res.* **9**, 4709–4719 (1981).
34. Reiter, H., Milewskiy, M. & Kelley, P. Mode of action of phleomycin on Bacillus subtilis. *J. Bacteriol.* **111**, 586–592 (1972).
35. Liu, L. F. *et al.* Mechanism of action of camptothecin. *Ann. N. Y. Acad. Sci.* **922**, 1–10 (2000).
36. Chabanon, R. M. *et al.* PBRM1 Deficiency Confers Synthetic Lethality to DNA Repair Inhibitors in Cancer. *Cancer Res.* **81**, 2888–2902 (2021).
37. Van Nuland, R. *et al.* Nucleosomal DNA binding drives the recognition of H3K36-methylated nucleosomes by the PSIP1-PWWP domain. *Epigenetics and Chromatin* **6**, 1–12 (2013).
38. Herrera-Moyano, E., Mergui, X., García-Rubio, M. L., Barroso, S. & Aguilera, A. The yeast and human FACT chromatin-reorganizing complexes solve R-loop-mediated transcription-replication conflicts. *Genes Dev.* **28**, 735–748 (2014).
39. Promonet, A. *et al.* Topoisomerase 1 prevents replication stress at R-loop-enriched transcription termination sites. *Nat. Commun.* **11**, 1–12 (2020).
40. Zatreanu, D. *et al.* Elongation Factor TFIIS Prevents Transcription Stress and R-Loop Accumulation to Maintain Genome Stability. *Mol. Cell* **76**, 57-69.e9 (2019).

41. Laspata, N. *et al.* PARP1 associates with R-loops to promote their resolution and genome stability. *Nucleic Acids Res*. **51**, 2215–2237 (2023).
42. Lin, W.-L. *et al.* DDX18 prevents R-loop-induced DNA damage and genome instability via PARP-1. *Cell Rep*. **40**, 111089 (2022).
43. Daugaard, M. *et al.* Lens epithelium-derived growth factor is an Hsp70-2 regulated guardian of lysosomal stability in human cancer. *Cancer Res.* **67**, 2559–2567 (2007).
44. Alonso, M. S. M. & Noordermeer, S. M. Untangling the crosstalk between BRCA1 and R-loops during DNA repair. *Nucleic Acids Res*. **49**, 4848–4863 (2021).
45. Katyal, S. *et al.* Aberrant topoisomerase-1 DNA lesions are pathogenic in neurodegenerative genome instability syndromes. *Nat. Neurosci.* **17**, 813–821 (2014).
46. Ye, B. J., Kang, H. J., Lee-Kwon, W., Kwon, H. M. & Choi, S. Y. PARP1-mediated PARylation of TonEBP prevents R-loop-associated DNA damage. *DNA Repair (Amst).* **104**, (2021).
47. Zhao, J. *et al.* A PARylation-phosphorylation cascade promotes TOPBP1 loading and RPA-RAD51 exchange in homologous recombination. *Mol. Cell* **82**, 2571-2587.e9 (2022).
48. Li, X. & Manley, J. L. Inactivation of the SR protein splicing factor ASF/SF2 results in genomic instability. *Cell* **122**, 365–378 (2005).
49. Pradeepa, M. M., Sutherland, H. G., Ule, J., Grimes, G. R. & Bickmore, W. A. Psip1/Ledgf p52 binds methylated histone H3K36 and splicing factors and contributes to the regulation of alternative splicing. *PLoS Genet.* **8**, e1002717 (2012).
50. Niehrs, C. & Luke, B. Regulatory R-loops as facilitators of gene expression and genome stability. *Nature Reviews Molecular Cell Biology* vol. 21 167–178 (2020).
51. Svejstrup, J. Q. The interface between transcription and mechanisms maintaining genome integrity. *Trends Biochem. Sci.* **35**, 333–338 (2010).
52. Tan-Wong, S. M., Dhir, S. & Proudfoot, N. J. R-Loops Promote Antisense Transcription across the Mammalian Genome. *Mol. Cell* **76**, 600-616.e6 (2019).
53. Yasuhara, T. *et al.* Human Rad52 Promotes XPG-Mediated R-loop Processing to Initiate Transcription-Associated Homologous Recombination Repair. *Cell* **175**, 558-570.e11 (2018).
54. Farmer, H. *et al.* Targeting the DNA repair defect in BRCA mutant cells as a therapeutic strategy. *Nature* **434**, 917–921 (2005).
55. Ngo, G. H. P., Grimstead, J. W. & Baird, D. M. UPF1 promotes the formation of R loops to stimulate DNA double-strand break repair. *Nat. Commun. 2021 121* **12**, 1–15

(2021).

Acknowledgements
We thank QMUL epigenetics hub members and Madapura lab members for discussing and reading the manuscript. We thank Vaclav Veverka (Charles University, Czech Republic) for sharing recombinant PSIP1 proteins, Francisco Martin-Zamora and Chema Martin (QMUL) lab for sharing purified pATn5, Martin Regins (MRC-HGU, Edinburgh) for RNASEH1 plasmid, Benjamin JE Martin (Harvard Medical School) for TT-seq protocol. We thank Blizard core facilities and Luke Gammon, Maeve McLaughlin and Gary Warnes for their help in image analysis training and FACS analysis. This research utilised Queen Mary's Apocrita HPC facility, supported by QMUL Research-IT.

Funding: Marie Skłodowska-Curie Actions Individual Fellowship (896079-JS), Medical Research Council UKRI/MRC grant and Barts charity grant (MR/T000783/1; MGU0475-MMP).

Author contributions:

Conceptualisation: MMP, JS, HT

Methodology: MMP, JS, HT, MP, GB, FB

Investigation: MMP, JS, MP, HA

Visualisation: MMP, JS, MP,

Funding acquisition: MMP, JS,

Project administration: MMP

Supervision: MMP, HT

Writing – original draft: MMP, JS,

Writing – review & editing: MMP, JS, HT, MP, GB

Competing interests: Authors declare that they have no competing interests.

Figure Legends

Figure 1. PSIP1 depletion leads to the accumulation of R-loops.

a) Schematic showing PSIP1 domains, shRNA targeting region and antibody epitope used in the study. **b**) Immunofluorescence (IF) images and dot plot of γ-H2AX foci in wild-type, *Psip1*$^{-/-}$ and *Psip1*$^{-/-}$ p75R MEFs (representative images; n>1500 nuclei observed over three independent experiments; median values indicated with red bar; p values obtained using two-tailed Mann-Whitney test). **c**) Slot blot images showing the binding of p75/p52 isoforms of PSIP1 with RNA-DNA hybrids in the genomic DNA. RNASEH-treated genomic DNA and IgG served as a control. Normalised band intensity has been shown (right) with mean ± SD (n=3 independent experiments; P values by one-way ANOVA). **d**) Immunoblots of S9.6, H3 and IgG immunoprecipitated (IP) lysates from RWPE-1 cell nuclear extract with indicated antibodies. **e**) Representative images and dot plot showing PLA foci between S9.6 and PSIP1 in control and RNASEH1 overexpressed RWPE-1 cells (n>1400 nuclei observed over three independent experiments; median values indicated with red line; p values obtained using two-tailed Mann-Whitney test). **f**) Slot blot for R-loop using S9.6 antibody from cells as in **b**. Staining with methylene blue was used as loading control. The normalised band intensity (right) was plotted as mean ± SD (n=3 independent experiments; p values by one-way ANOVA). **g**) Immunoblot with PSIP1/p75 and β-actin for lysate from PSIP1-shRNA (PSIP1-sh) and non-targeting control shRNA (control-sh). **h**) S9.6 immunofluorescence in RWPE-1 cells (left) and quantification (representative images; n>4000 nuclei from three independent experiments; median values are indicated with the red line; p values by two-tailed Mann-Whitney test). **i**) Like **f**, but for PSIP1 knockdown (PSIP1-sh) and control knockdown (control-sh) RWPE-1 cells. R-loops isolated from cells overexpressing RNASEH1 also was used for slot blot. The normalised band intensity has been plotted as mean ± SD (n=3 independent experiments; p values by one-way ANOVA). **j**) Heatmaps showing E. coli spike-in normalised CUT&Tag reads for PSIP1/p75 in control and PSIP1 knockdown RWPE-1 cells. **k**) Heatmap showing R-loop and PSIP1/p75 levels in PSIP1-KD and control RWPE-1 cells. **l**) Genome browser track (hg38) showing the CUT&Tag signal (read counts) for PSIP1 and R-loop in control and PSIP1-KD RWPE-1 cells. Source data for this figure are provided as a Source Data file.

Figure 2. PSIP1 depletion leads to R-loop-mediated DNA damage.

a) Western blots showing the levels of γ-H2AX in control and PSIP1 KD RWPE-1 cells. **b**) Representative IF images and dot plot showing the γ-H2AX foci in control and PSIP1 KD RWPE-1 cells. The cells overexpressing RNASEH1 were also used as controls. The number of foci per cell was quantified and plotted as dot plot (n>8000 nuclei from three independent experiments; Median values are indicated with red line; p values by two-tailed Mann-Whitney test). **c**) Like **b** but for 53BP1 foci (representative images; n>3000 cells for each group from three independent experiments; median values are indicated with red bars; p values by two-tailed Mann-Whitney test). **d**) Immunoblot images showing the bulk levels of 53BP1 protein in control, PSIP1 KD and upon RNASEH1 overexpression in HEK293T cells. **e**) Heatmap showing CUT&Tag reads (normalised to E. coli reads) for γ-H2AX and PSIP1/p75 across S9.6 peaks gained in PSIP1-KD HEK293T cells. **f**) Genome-browser tracks showing CUT&Tag data for PSIP/p75, R-loops (S9.6 ab) and γ-H2AX in control and PSIP-

KD HEK293T cells. **g**) Representative images and dot plot of PLA between R-loops (S9.6) and γ-H2AX antibodies in control and PSIP-KD RWPE1 cells (representative images; n>1000 nuclei observed from three independent experiments; median values indicated with red bar; p values obtained using two-tailed Mann-Whitney test). Source data for this figure are provided as a Source Data file.

Figure 3. R-loop accumulation at promoters leads to transcription-replication conflict.

a) Distribution of PSIP1, R-loop (S9.6 ab), and γ-H2AX CUT&Tag peaks from RWPE-1 cells around the gene transcription start sites (promoters), gene bodies and intergenic regions. **b**) Heatmaps showing the log2 fold change in read counts between control and PSIP1-KD CUT&Tag reads for PSIP1/p75, R-loops (S9.6 ab) and γ-H2AX in RWPE-1 cells across the NCBI reference genes. **c**) upSet plot and Venn diagram (right) showing the unique and overlapping peaks obtained from CUT&Tag reads for PSIP1, S9.6 and γ-H2AX in HEK 293T cells. The X-axis shows the number of peaks, and the Y-axis shows the number of intersections. **d**) Average profile with SD (shaded regions of blue and red) of TT-seq (RPKM) across protein-coding genes (left), dotted box show promoter region and around the centre of the S9.6 peaks gained in PSIP KD RWPE-1 cells (right). **e**) Slot blot using S9.6 antibody in control and PSIP-KD RWPE-1 cells after treatment with transcriptional inhibitor (triptolide 50 nM; 36h), methylene blue staining of the same DNA served as a loading control. Normalised intensity of S9.6 intensities was plotted as mean ± SD (n=3 independent experiments; p values by one-way ANOVA). **f**) Representative PLA image between α-PCNA and α-RNAPII antibodies obtained from control and PSIP1 KD RWPE-1 cells (left). The number of PLA foci per cell observed between PCNA and RNAPII was quantified and plotted as dot blot (n>1000 cells over three independent experiments; red line shows the median value that has been indicated; p values obtained from two-tailed Mann-Whitney test). Source data for this figure are provided as a Source Data file.

Figure 4. PSIP depletion leads to reduced HR repair at the R-loop-induced DNA damage.

a) Mean % survival ± SD of PSIP-KD and control-KD RWPE-1 cells treated with different concentrations of illudin-S, etoposide and aphidicolin drugs (n=3 independent experiments; p values by multiple unpaired t-tests). **b**) Western blot for γ-H2AX and DNA-PK (right) in control KD and PSIP1-KD cells in cells treated with phleomycin (1μg/ml) followed by repair for the indicated time. β-actin served as a loading control. **c**) Western blots for PSIP1/p75, γ-H2AX, for γ-H2AX IPed HEK293T extracts in control, PSIP1 KD, in the presence of camptothecin (CPT@10 μM; 2 h) (+) and DMSO (–). γ-H2AX IP was also performed after overexpressing the cells with RNASEH1. IgG is a negative control; input extracts are blotted (below). **d**) Representative immunofluorescence microscopic images showing 53BP1 foci in DMSO-treated or CPT (10μM; 2 h) treated RWPE-1 cells. The median and number of foci per cell are plotted as dot plot (n > 6000 cells in each group over three independent experiments; median values are indicated with red line and p values are obtained using two-tailed Mann-Whitney test). **e**) Like (**d**), but for RAD51 foci. Dot plots showing number of foci per cell with median values indicated (n > 6000 cells in each group over three independent experiments; p values obtained by two-tailed Mann-whitney test). Source data for this figure are provided as a Source Data file.

Figure 5. PSIP1 deficiency increases the sensitivity of cancer cells to drugs that induce transcription-coupled DNA damage.

a) Western blotting of S9.6, H3 and IgG immunoprecipitated (IP) from RWPE-1 cell nuclear extract with PSIP1/p75, PARP1, γ-H2AX and PCNA (negative control) antibodies. Lysate

treated with RNASEH before the pulldown was used as a negative control. IgG and H3 IP were negative controls, and 5% of the nuclear extract was used as input. **b**) Western blotting for PSIP1-IP with PSIP1, PARP1, γ-H2AX and PCNA antibodies, IgG served as a negative control. 10% of the nuclear extract was used as input. **c**) Western blotting for eGFP-PARP1 and HA-PSIP1 co-IPs performed using GFP-trap beads. αGFP ab was to detect eGFP-PARP1 and αHA to detect HA-PSIP1/p75 and HA-p52, along with γ-H2AX and PCNA antibodies. **d**) TGCA expression data showing levels of PSIP1 transcripts in cancers of the bladder (BLCA; n=408), breast (BRCA; n=1097), cervical (CESC; n=305), kidney chromophobe (KICH; n=67), kidney renal clear cell (KIRC; n=533), Kidney renal papillary cell (KIRP; n=290), lung (LUAD; n=515), lung squamous cell (LUSC; n=503), pancreatic (PAAD; n=178) and prostate (PRAD; n=497). The data was obtained from UALCAN online tool. The center line indicates a median value; the boxes and whiskers indicate 25th to 75th and 10th to 90th percentiles, respectively. **e**) Western blot showing the levels of PSIP1 in prostate normal and cancer cells and their sensitivity to olaparib as determined by CCK-8 assay (**f**). Mean survival ± SD is plotted (n=3 independent experiments). **g**) Western blot confirming the depletion of PSIP1 by shRNA in LNCaP cells **h**) Cell survival assay showing % survival of control and PSIP1 knockdown LNCaP cells with indicated doses of olaparib determined using the CCK-8 assay (mean ± SD; n=3 independent experiments). **i**) Similar to **h** but for indicated doses of illudin-S. **j**) Working model showing the role of PSIP1 in reducing R-loop level at transcription sites to minimise transcription-replication conflict leading to DNA damage. Source data for this figure are provided as a Source Data file.

Supplementary file includes
Supplementary figures 1 to 6
Supplementary legends 1to 6
Supplementary tables 1 and 2

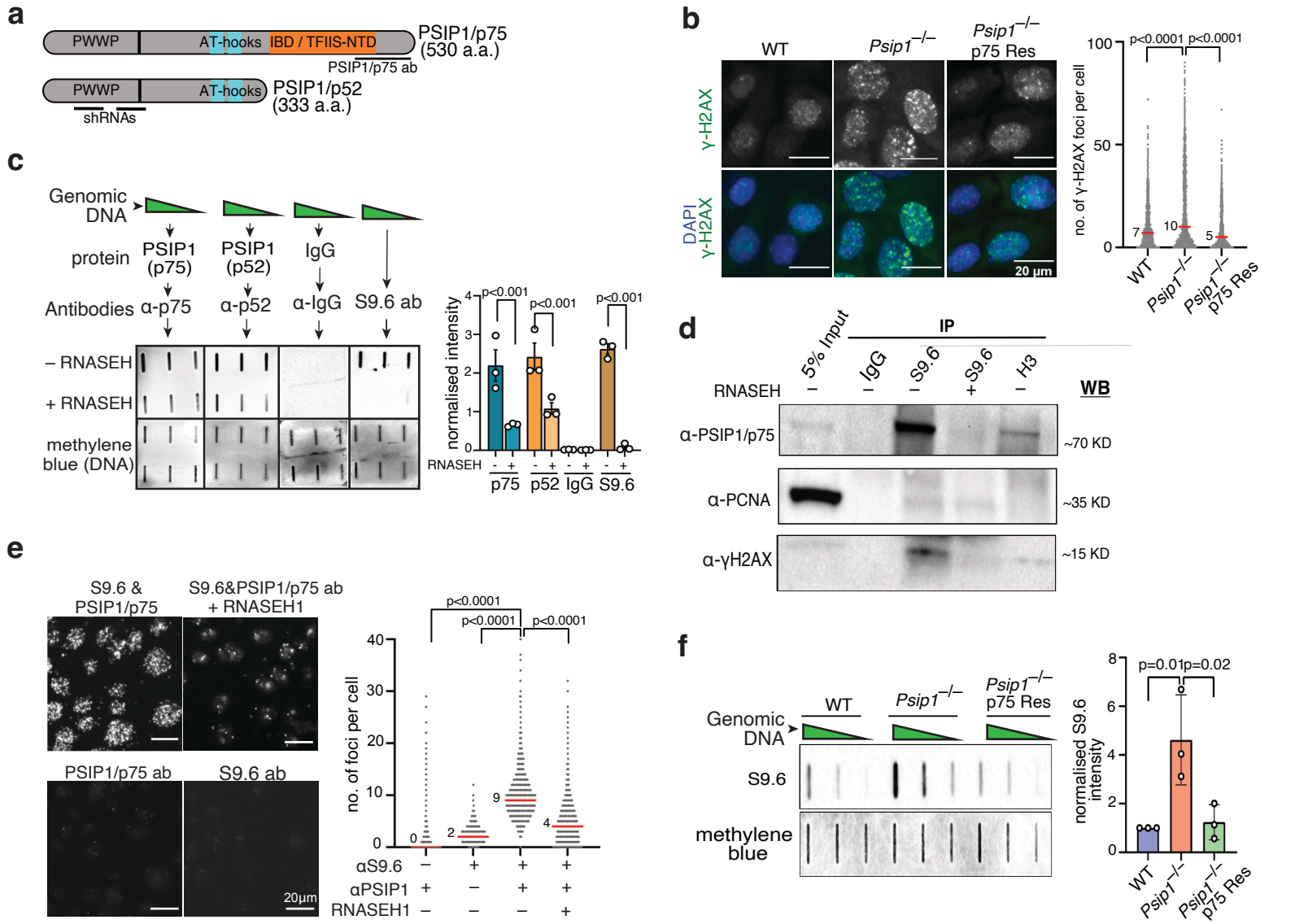
a
PWWP
AT-hooks
IBD / TFIIS-NTD
PSIP1/p75 (530 a.a.)
PSIP1/p75 ab
PWWP
AT-hooks
PSIP1/p52 (333 a.a.)
shRNAs
b
WT
Psip1−/−
Psip1−/− p75 Res
γ-H2AX
DAPI γ-H2AX
20 µm
no. of γ-H2AX foci per cell
p<0.0001
p<0.0001
7
10
5
c
Genomic DNA
protein
PSIP1 (p75)
PSIP1 (p52)
IgG
Antibodies
α-p75
α-p52
α-IgG
S9.6 ab
– RNASEH
+ RNASEH
methylene blue (DNA)
normalised intensity
p<0.001
p<0.001
p<0.001
RNASEH
p75
p52
IgG
S9.6
d
5% Input
IP
IgG
S9.6
S9.6
H3
RNASEH
WB
α-PSIP1/p75
α-PCNA
α-γH2AX
~70 KD
~35 KD
~15 KD
e
S9.6 & PSIP1/p75
S9.6&PSIP1/p75 ab + RNASEH1
PSIP1/p75 ab
S9.6 ab
20µm
no. of foci per cell
p<0.0001
p<0.0001
p<0.0001
0
2
9
4
αS9.6
αPSIP1
RNASEH1
f
WT
Psip1−/−
Psip1−/− p75 Res
Genomic DNA
S9.6
methylene blue
normalised S9.6 intensity
p=0.01
p=0.02
g
control-sh
PSIP1-sh
PSIP1
β-actin
~70 KD
~35 KD
h
– RNASEH1
+ RNASEH1
S9.6
DAPI
merge
cont-sh
PSIP1-sh
10µm
Nuclear levels of R-loops (arbitrary units)
p<0.0001
p<0.0001
545.6
499.1
707.7
556.2
RNASEH1
control-sh
PSIP1-sh
i
RNASEH
Genomic DNA
control-sh
PSIP1-sh
S9.6
methylene blue (DNA)
normalised S9.6 intensity
p=0.0081
p=0.013
RNASEH
cont-sh
PSIP1-sh
j
PSIP1/p75
cont-sh
PSIP1-sh
PSIP1 peaks in control-sh (n=2505)
-2.3K
center
2.3K
k
S9.6
PSIP1/p75
cont-sh
PSIP1-sh
cont-sh
PSIP1-sh
S9.6 peaks gained in PSIP1 KD (n=2741)
0
70
0
90
read counts/E. coli reads
l
chr5:171,390,000
S9.6
(cont-sh)
(PSIP1-sh)
PSIP1
(cont-sh)
(PSIP1-sh)
NPM1

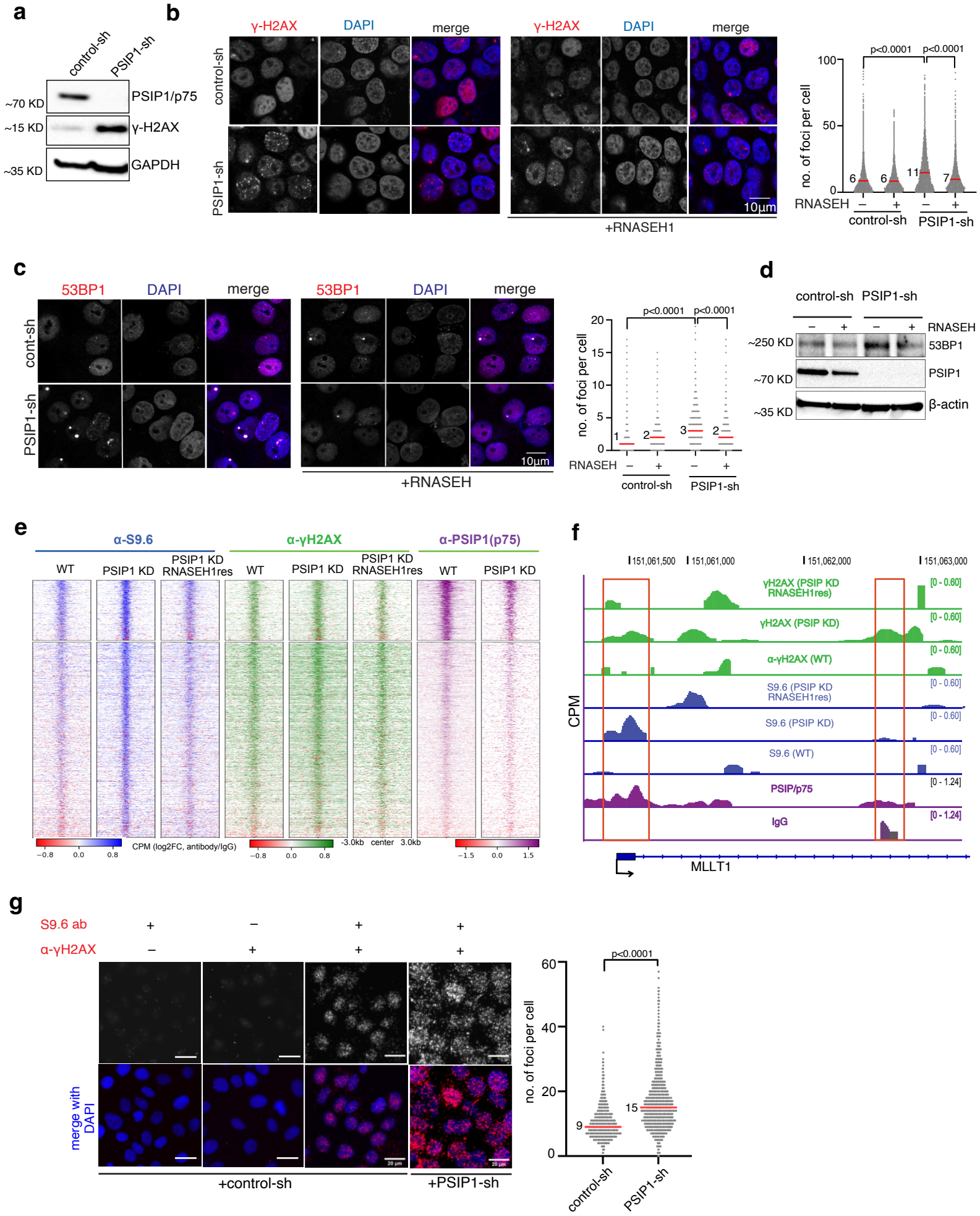
a
control-sh
PSIP1-sh
~70 KD
~15 KD
~35 KD
PSIP1/p75
γ-H2AX
GAPDH
b
γ-H2AX
DAPI
merge
control-sh
PSIP1-sh
10μm
+RNASEH1
p<0.0001
p<0.0001
no. of foci per cell
RNASEH
control-sh
PSIP1-sh
c
53BP1
DAPI
merge
cont-sh
PSIP1-sh
10μm
+RNASEH
p<0.0001
p<0.0001
no. of foci per cell
RNASEH
control-sh
PSIP1-sh
d
control-sh
PSIP1-sh
RNASEH
~250 KD
~70 KD
~35 KD
53BP1
PSIP1
β-actin
e
α-S9.6
α-γH2AX
α-PSIP1(p75)
WT
PSIP1 KD
PSIP1 KD RNASEH1res
CPM (log2FC, antibody/IgG)
-3.0kb
center
3.0kb
f
151,061,500
151,061,000
151,062,000
151,063,000
γH2AX (PSIP KD RNASEH1res)
γH2AX (PSIP KD)
α-γH2AX (WT)
S9.6 (PSIP KD RNASEH1res)
S9.6 (PSIP KD)
S9.6 (WT)
PSIP/p75
IgG
CPM
MLLT1
g
S9.6 ab
α-γH2AX
merge with DAPI
+control-sh
+PSIP1-sh
p<0.0001
no. of foci per cell
control-sh
PSIP1-sh

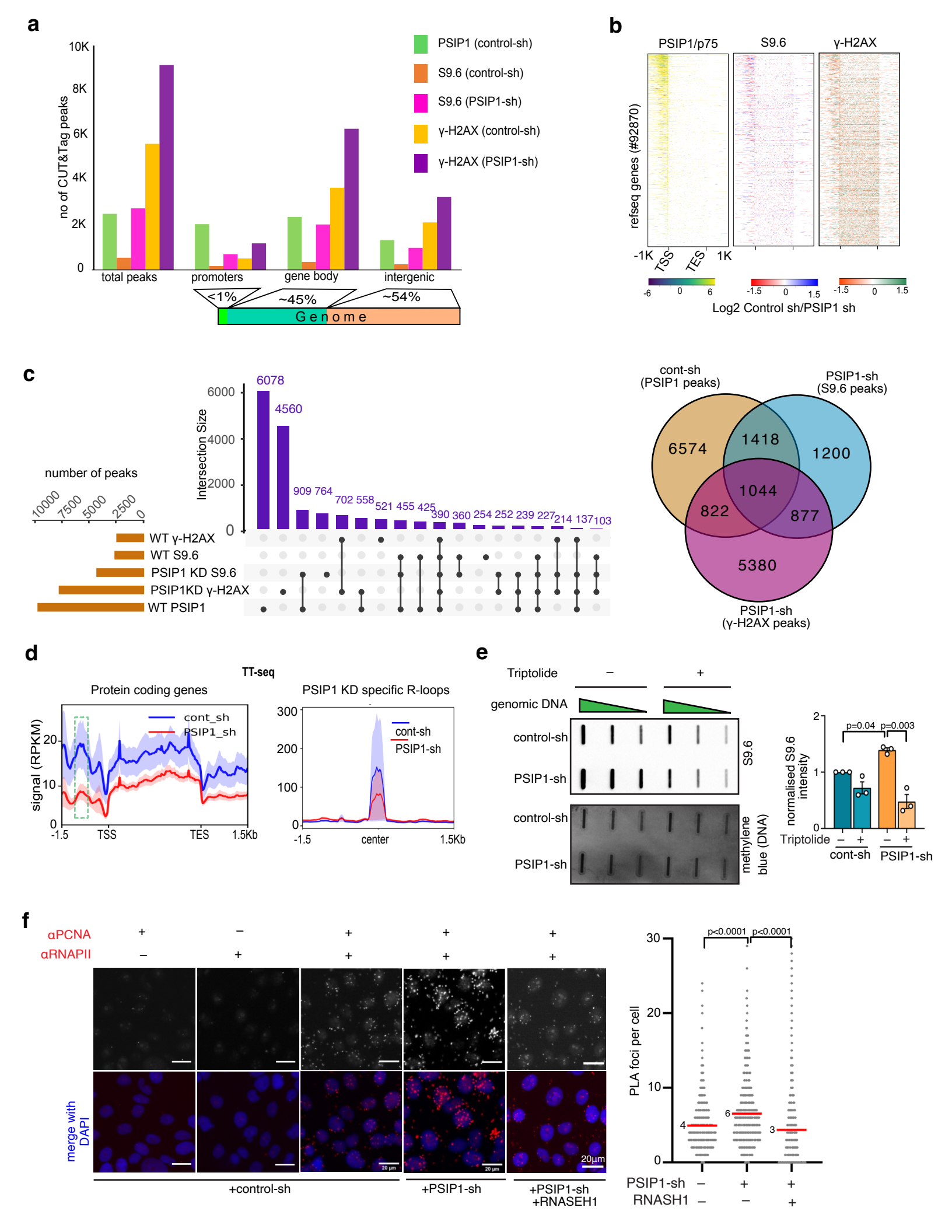
a
no of CUT&Tag peaks
10K
8K
6K
4K
2K
0
PSIP1 (control-sh)
S9.6 (control-sh)
S9.6 (PSIP1-sh)
γ-H2AX (control-sh)
γ-H2AX (PSIP1-sh)
total peaks
promoters
gene body
intergenic
<1%
~45%
~54%
Genome
b
PSIP1/p75
S9.6
γ-H2AX
refseq genes (#92870)
-1K
TSS
TES
1K
-6
0
6
-1.5
0
1.5
Log2 Control sh/PSIP1 sh
c
Intersection Size
6000
4000
2000
0
6078
4560
909 764
702 558
521 455 425
390 360 254 252 239 227 214 137 103
number of peaks
10000
7500
5000
2500
0
WT γ-H2AX
WT S9.6
PSIP1 KD S9.6
PSIP1KD γ-H2AX
WT PSIP1
cont-sh
(PSIP1 peaks)
PSIP1-sh
(S9.6 peaks)
PSIP1-sh
(γ-H2AX peaks)
6574
1418
1200
1044
822
877
5380
d
TT-seq
Protein coding genes
PSIP1 KD specific R-loops
signal (RPKM)
cont_sh
PSIP1_sh
-1.5
TSS
TES
1.5Kb
cont-sh
PSIP1-sh
center
e
Triptolide
–
+
genomic DNA
control-sh
PSIP1-sh
S9.6
methylene blue (DNA)
normalised S9.6 intensity
p=0.04
p=0.003
cont-sh
PSIP1-sh
f
αPCNA
αRNAPII
merge with DAPI
20μm
+control-sh
+PSIP1-sh
+PSIP1-sh
+RNASEH1
PLA foci per cell
p<0.0001
p<0.0001
PSIP1-sh
RNASH1

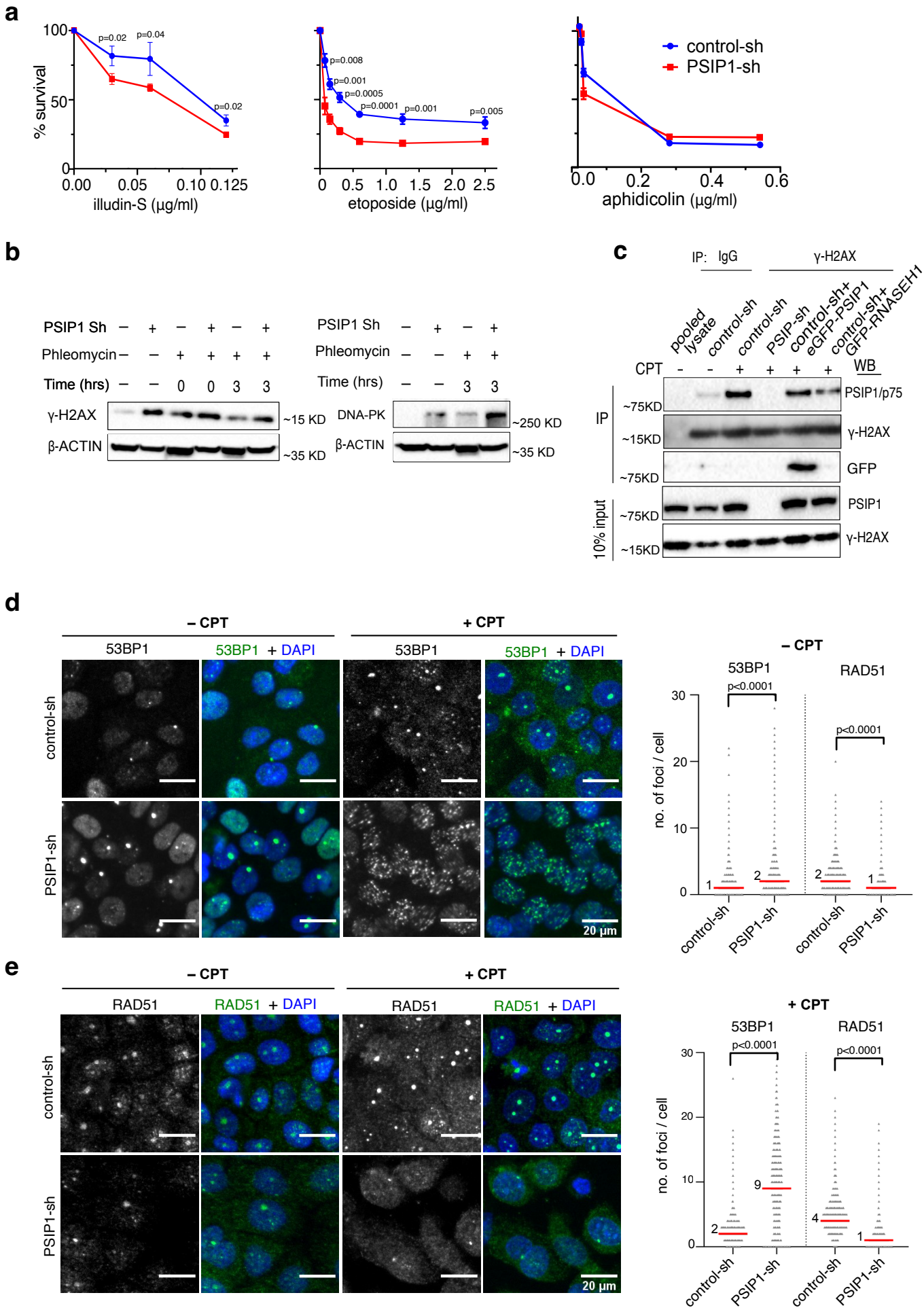
a
% survival
illudin-S (µg/ml)
etoposide (µg/ml)
aphidicolin (µg/ml)
control-sh
PSIP1-sh
p=0.02
p=0.04
p=0.008
p=0.001
p=0.0005
p=0.0001
p=0.005
b
PSIP1 Sh
Phleomycin
Time (hrs)
γ-H2AX
β-ACTIN
~15 KD
~35 KD
DNA-PK
~250 KD
c
IP: IgG
γ-H2AX
pooled lysate
control-sh
PSIP-sh
control-sh+ eGFP-PSIP1
control-sh+ GFP-RNASEH1
CPT
WB
IP
10% input
~75KD
~15KD
PSIP1/p75
GFP
PSIP1
d
– CPT
+ CPT
53BP1
53BP1 + DAPI
control-sh
PSIP1-sh
20 µm
RAD51
no. of foci / cell
p<0.0001
e
RAD51
RAD51 + DAPI

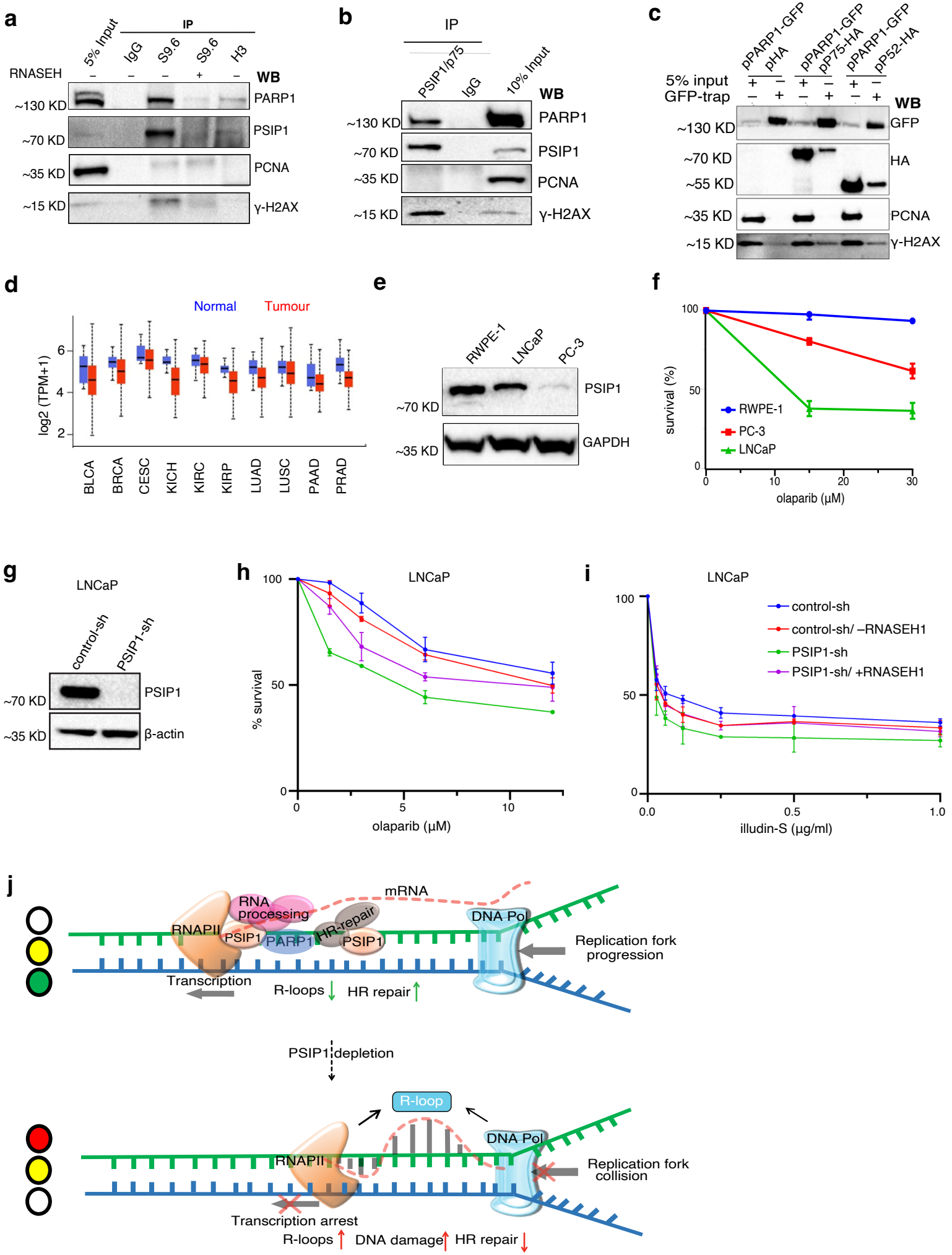
a
5% Input
IP
IgG
S9.6
S9.6
H3
RNASEH
–
–
–
+
–
WB
~130 KD
PARP1
~70 KD
PSIP1
~35 KD
PCNA
~15 KD
γ-H2AX
b
IP
PSIP1/p75
IgG
10% Input
WB
~130 KD
PARP1
~70 KD
PSIP1
~35 KD
PCNA
~15 KD
γ-H2AX
c
pPARP1-GFP
pHA
pPARP1-GFP
pP75-HA
pPARP1-GFP
pP52-HA
5% input
GFP-trap
WB
~130 KD
GFP
~70 KD
HA
~55 KD
~35 KD
PCNA
~15 KD
γ-H2AX
d
Normal
Tumour
log2 (TPM+1)
BLCA
BRCA
CESC
KICH
KIRC
KIRP
LUAD
LUSC
PAAD
PRAD
e
RWPE-1
LNCaP
PC-3
~70 KD
PSIP1
~35 KD
GAPDH
f
survival (%)
RWPE-1
PC-3
LNCaP
olaparib (μM)
g
LNCaP
control-sh
PSIP1-sh
~70 KD
PSIP1
~35 KD
β-actin
h
LNCaP
% survival
olaparib (μM)
i
LNCaP
control-sh
control-sh/ –RNASEH1
PSIP1-sh
PSIP1-sh/ +RNASEH1
illudin-S (μg/ml)
j
mRNA
RNA processing
RNAPII
PSIP1
PARP1
HR-repair
PSIP1
DNA Pol
Replication fork progression
Transcription
R-loops
HR repair
PSIP1 depletion
R-loop
RNAPII
DNA Pol
Replication fork collision
Transcription arrest
R-loops
DNA damage
HR repair